Superconductor Science and Technology

PAPER • OPEN ACCESS

Superconducting low-beta Nb_3Sn cavity for ATLAS and future ion accelerators

To cite this article: T Petersen *et al* 2026 *Supercond. Sci. Technol.* **39** 045006

IOP Publishing Supercond. Sci. Technol. 39 (2026) 045006 https://doi.org/10.1088/1361-6668/ae54d8

Superconductor Science and Technology

Check for updates

OPEN ACCESS

RECEIVED
30 October 2025

REVISED
13 February 2026

ACCEPTED FOR PUBLICATION
18 March 2026

PUBLISHED
10 April 2026

PAPER

Superconducting low-beta Nb_3Sn cavity for ATLAS and future ion accelerators

T Petersen[1,4,*], G Eremeev[2,4], B Tennis[2], N Tagdulang[2], Y Zhou[1], M Kedzie[1], B Guilfoyle[1], S Xu[1,5], S V Kutsaev[3], R Agustsson[3], E Spranza[3], P Davis[1], G P Zinkann[1], T Reid[1], S Posen[2] and M P Kelly[1]

[1] Argonne National Laboratory, Lemont, IL, United States of America
[2] Fermi National Accelerator Laboratory, Batavia, IL, United States of America
[3] RadiaBeam Technologies, Santa Monica, CA, United States of America
[4] These authors contributed equally to this work.
[5] University of California, Davis, Davis, United States of America.
[*] Author to whom any correspondence should be addressed.

E-mail: tpetersen@anl.gov

Keywords: SRF, low-beta accelerator, thin films, Nb_3Sn, accelerators, quarter wave resonator

Supplementary material for this article is available online

Abstract

We report on a Nb_3Sn-coated low-beta superconducting radio frequency (RF) cavity intended for accelerating ions. We aim to apply the cavity in ATLAS, our Argonne National Laboratory user facility for nuclear physics studies with ion beams in the energy range of 5–20 MeV u^{-1}. The Nb_3Sn-coated cavity, a 145 MHz quarter-wave optimized for ions moving with velocity $\beta = v/c = 0.08$ exhibits an order-of-magnitude reduction in RF losses into helium at 4.4 K compared to a superconducting niobium (Nb) cavity at the same frequency and temperature. Experimentally measured fields are among the highest to date for any Nb_3Sn-coated cavity, reaching a peak surface magnetic field of 105 mT. We also present a practical solution to the problem of cavity frequency tuning. Tuning by mechanical deformation has been a challenge with Nb_3Sn due to its brittle nature, however, using a set of techniques tailored to the properties of thin-film Nb_3Sn on Nb, we can repeatably tune the cavity to the ATLAS master clock frequency after it is cooled, while maintaining the excellent performance characteristics. The same Nb_3Sn cavity technology offers broad benefits for future ion accelerators.

1. Introduction

Superconducting cavities are the leading technology for a large class of particle accelerators requiring proton and ion beams with energies from 5 MeV u^{-1} to 2.5 GeV u^{-1} or higher [1–5]. Their distinguishing attribute is their ability to support high accelerating gradients in continuous wave operation. Other beneficial properties include large transverse apertures and broad particle velocity acceptance. Well-developed ion linac cavity types include quarter-wave, half-wave and elliptical shapes, with the optimal type determined primarily by the ion velocity [6]. Cavities are arranged in fixed linear arrays, and the short (∼1 m long) independently controlled cavities permit the acceleration of ions with variable energy over a wide range of mass-to-charge (e.g. $1 \leqslant A/q \leqslant 7$). This is essential for accelerators, such as ATLAS, that must deliver different ion species at variable energies.

We are developing a 145 MHz Nb_3Sn-coated quarter-wave cavity as a path to overcoming the performance limits of existing ATLAS Nb cavities. The development builds on prior work with a 218 MHz prototype cavity [7]. Nb_3Sn has roughly twice the critical temperature of Nb ($T_c = 18$ K vs 9.2 K) and nearly twice the superheating field ($H_{SH} \approx 400$ mT vs 240 mT) [8, 9]. Because the Bardeen–Cooper–Schrieffer (BCS) portion of the cavity surface resistance, R_{BCS}, decreases exponentially with temperature for $T \lesssim T_c/2$ [10–12], the higher T_c for Nb_3Sn makes it possible to achieve more than an order of magnitude reduction in radio frequency (RF) losses with Nb_3Sn at 4.4 K. H_{SH} is thought to present the fundamental limit on the highest sustainable magnetic field for superconducting RF (SRF) cavities, meaning that Nb_3Sn also offers the possibility for higher accelerating gradients.

ATLAS beam physics requirements, set by the 49 operating Nb cavities, confine us to 50–150 MHz. However, we expect that the optimal frequencies for future 'green-field' Nb_3Sn-based ion linacs will be higher (e.g. 500 MHz), stemming from the expected R_{BCS} frequency and temperature dependence for Nb_3Sn [9]. This would greatly reduce quarter- and half-wave (TEM-mode) cavity size and cost. At the same time, the reduction in RF power losses into helium at 4.4 K would enable the use of small, plug-in cryocoolers in place of large central liquid helium cryoplants and their complex distribution systems [13, 14]. This prospect has motivated Nb_3Sn development for elliptical cavities for particles with $\beta \approx 1$ [15–17].

2. Experimental approach

Electromagnetic (EM) simulations of the 145 MHz quarter-wave cavity RF volume and access ports were performed using CST Microwave Studio. Results for electric and magnetic fields and primary EM design parameters for the accelerating mode are in figure 1 and table 1. Arrow sizes and directions in figure 1 indicate the relative strength and direction of the fields. The cavity shape includes the quarter-wave beam steering correction [18] and is generally similar to that for lower frequency niobium cavities operating in ATLAS. Conway *et al* [19] Mechanical design and stress analyses were performed using COMSOL and AutoDesk Inventor.

The physical Nb_3Sn-coated cavity was formed starting from a Nb cavity fabricated by RadiaBeam and Argonne from high-purity (residual resistivity ratio, $RRR > 250$) 3 mm-thick Nb sheet using well-developed techniques including die hydroforming, CNC machining, wire electron discharge machining and electron beam welding. Re-enforcing plates on the top and bottom of the cavity and flanges on the access ports were from lower-purity Nb ($RRR \approx 50$) and a Nb (55%)-titanium alloy, respectively. The interior surface of the Nb cavity was prepared for coating by removing 120 μm of niobium by electropolishing, similar as for standard Nb cavities. Ultrasonic and high-pressure water cleaning were used to remove chemical residues.

A ∼2 μm-thick Nb_3Sn layer was formed on the cavity RF surface at Fermilab by vapor diffusion in a high-vacuum furnace at 1100 °C. Procedures to minimize contamination of the Nb_3Sn layer during coating-particularly from NbTi flanges-follow established best practices for elliptical-cell cavities [9, 20](including covering NbTi flanges with niobium covers and foils as best as possible). In the absence of prior low-beta experience with Nb_3Sn coatings, we adopted the elliptical-cell protocol with geometry-specific adaptations. The cavity was mounted with the long axis horizontal in the vacuum furnace, as in figure 2(left image), with a two tin/tin-chloride ($Sn/SnCl_2$) sources fixed to two of the six cavity ports. After the 218 MHz coating, the location for the tin sources was optimized to provide line of sight to the high magnetic field region of the cavity, as shown in figure 3. Nb covers and foils, used to cover NbTi flanges, received light chemistry to remove contamination, which is evidenced by discoloration observed on the surfaces facing NbTi. The furnace containing the cavity, tin sources and heater assemblies, was ramped to 1100 °C while the wire-heaters elevated the source temperatures to 1300 °C. The latter increases the tin vapor pressure inside the cavity helps promote stoichiometric A15 growth. The coated cavity was cooled under vacuum to 50 °C before venting with dry nitrogen and removal from the furnace.

Final cleaning of the coated Nb_3Sn cavity was similar to that for niobium cavities. High-pressure water rinsing with ultrapure water, clean room assembly, and a slow controlled pump down of the interior volume were used to minimize particulate contamination. During clean assembly the cavity was fitted with fixed RF drive and pickup probes with Q_{ext} values of 9.5×10^9 and 2.9×10^{11} respectively. Performance of the cavity at 4.4 K was measured before and after coating, to ensure that coating was on top of niobium of known good performance. All cold testing was performed by fully immersing the sealed and vertically oriented cavity into a bath of liquid helium contained inside a 60 cm diameter vacuum insulated and liquid nitrogen shielded dewar filled to a level of ∼90 cm. The helium bath pressure was maintained in the range of 1000 ± 50 Torr, with an associated helium bath temperature of 4.45 ± 0.05 K.

Cavity performance was measured as described in [11]. Continuous-wave RF power from a few μW to 17.5 W (coupled into the cavity) was delivered via the drive probe, with a phase-locked loop maintaining constant field. The power coupled into the cavity was taken as $P_{in} = P_{fwd} - P_{refl}$, with P_{fwd} and

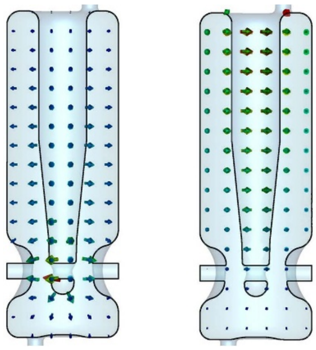

Figure 1. Cavity section views showing electric (left) and magnetic (right) fields from CST MWS.

Table 1. Primary cavity electromagnetic and mechanical properties.

Parameter	Value	Unit
Frequency	145.492	MHz
Peak beta	0.08	
R/Q	433	Ohms
G	29.5	Ohms
Beam aperture	3	cm
Diameter	21.6	cm
Height	63	cm
Design voltage	1.33	MV
At the design voltage		
Stored energy	4.5	Joules
E_{PEAK}	51.6	$MV\,m^{-1}$
B_{PEAK}	60	mT

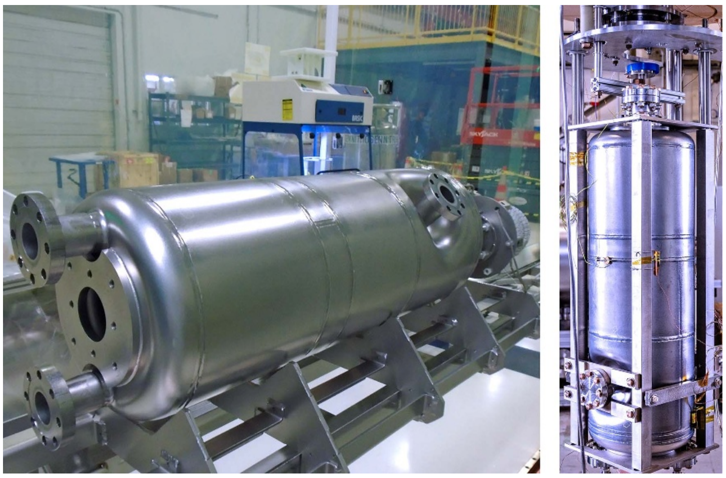

Figure 2. Cavity with Sn source assembly after furnace coating (left) and cavity with Ti frame (right).

P_{refl} being the forward and reflected RF power measured via dual directional coupler. The cavity Q_0 and E_{acc} were then obtained from the measured input and pickup couplings, the RF decay time τ, and the CST MWS-simulated relation between stored energy U and accelerating gradient E_{acc}.

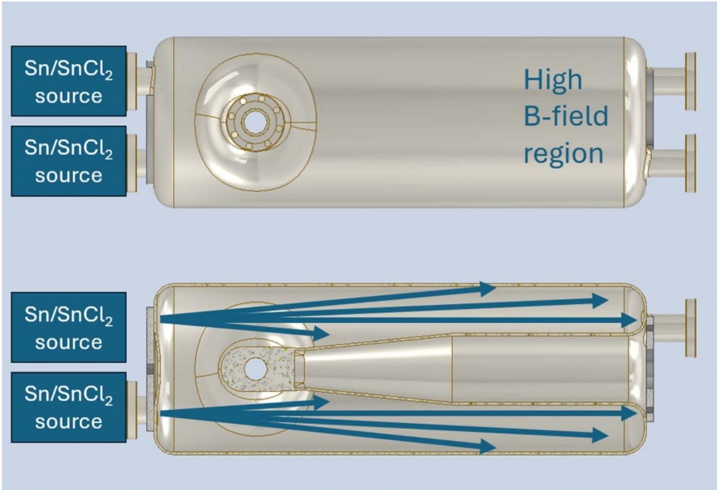

Figure 3. Section view schematic showing tin sources and line of sight to high magnetic field region.

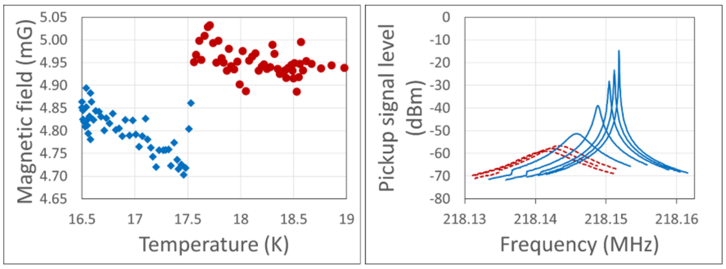

Figure 4. T_c measurement for 218 MHz cavity. Magnetic field data (left) and VNA S_{21} data (right).

3. Field performance results

The superconducting transition temperature was $T_c = 17.7 \pm 0.1$ K, determined primarily from VNA measurements of the cavity S_{21} resonance at low forward power; temperature was read from silicon-diode thermometers distributed from top to bottom of the cavity. Magnetic flux expulsion-evidenced by a stepwise change in the local B field measured by three Bartington fluxgate magnetometers on the cavity exterior-occurred at the same temperature.

Concurrent magnetic field and temperature data were collected during both 218 MHz and 145 MHz QWR tests. VNA measurements of S_{21} at very low power ($\leqslant$10 mW) were also made for each case. The instrument bandwidth of 10 Hz precluded a precise Q measurement in the superconducting state. However, tracking the resonance does provide a clear albeit semi-quantitative measurement of the Q change, that combined with the magnetic field and temperature data, give an error in the T_c measurement of no more than $\pm$0.1 K.

A calibrated ($\pm$12 mK) DT-670 diode was added to the later 145 MHz tests. Two magnetic field compensation coils were used to reduce the ambient magnetic field at the cavity to a value of $\leqslant$10 mG. Figures 4 and 5 show temperatures of superconducting transition for the 218 MHz and 145 MHz cavities, respectively. The 218 MHz magnetic field measurement was made with the field probe near the toroid, while the 145 MHz had three probes across the cavity.

Figure 6 compares 4.4 K performance before and after coating. The lowest curve is for the uncoated Nb cavity. The first test of the Nb_3Sn-coated cavity (middle curve) exhibited a high cavity quality factor at low fields, with $Q > 10^{10}$, a high maximum accelerating gradient, $E_{acc} = 12.5$ MV m^{-1}, (B_{PEAK} = 95 mT), but also, a pronounced downward slope in the quality factor with increasing gradient. The relative improvement in cavity Q after Nb_3Sn coating compared to the Nb cavity was one order of magnitude at very low fields; however, this decreased to a factor of 3 for $E_{acc} \geqslant 1$ MV m^{-1}.

'Q-slope' can arise from several mechanisms, notably electron field emission (FE) and magnetic flux trapping [21–23]. We rule out a substantial contribution from FE based on the lack of detectable

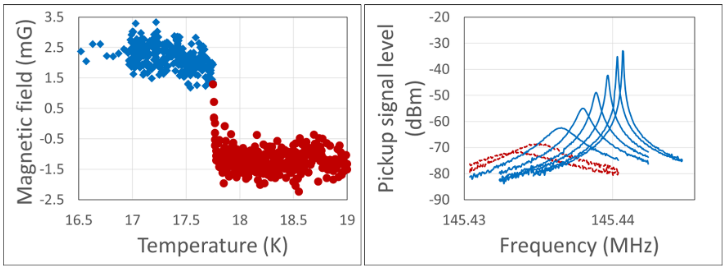

Figure 5. T_c measurement for 145 MHz cavity. Magnetic field data (left) and VNA S_{21} data (right).

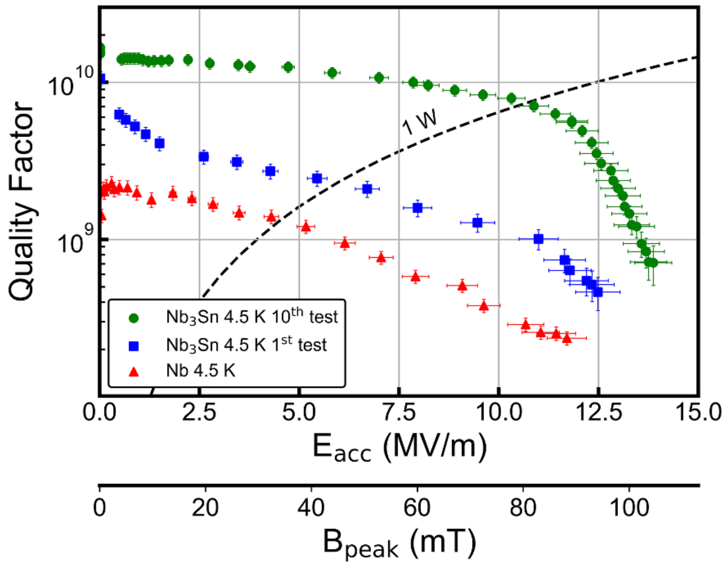

Figure 6. Cavity Q versus accelerating gradient and peak magnetic field. 1 W constant transmitted power line shown for reference.

x-rays at the Geiger–Müeller detector placed 40 cm from the cavity wall on the outside of the cryostat. Maximum ambient (residual Earth's) magnetic fields over the volume of the cavity were 10 mG, as measured by three fluxgate magnetometers mounted inside the helium cryostat and against the cavity outer wall. In the worst case of 100% flux trapping with $B_{\mathrm{ambient}} = 10$ mG and using $R_s = 0.2\,\mathrm{n}\Omega\,\mathrm{mG}^{-1}$ [24, 25] the added residual resistance would be 2 nΩ. With geometry factor $G = Q_0 R_s = 29.5\ \Omega$, this implies $Q_0 \gtrsim G/R_s \approx 1.48 \times 10^{10}$, i.e. slightly higher than the low field Q but much higher than the Q at high fields for this first test. This pointed to the possibility of trapped magnetic flux as the issue.

Magnetic fields from Seebeck-driven thermocurrents near T_c can degrade Q_0 of Nb_3Sn cavities [26]. In a 218 MHz Nb_3Sn quarter-wave cavity, cooling through T_c at a rate of $1\,\mathrm{mK\,s^{-1}}$ or slower with a maximum temperature gradient $\Delta T \sim 200$ mK minimized the Q_0 degradation due to thermocurrents. For the initial 145 MHz assembly, multiple warm/cool cycles through T_c produced only minor changes in the Q_0 versus E_{ACC} relative to the large overall Q-slope. These results suggest that the Q-slope is not primarily caused by residual Earth's field or thermocurrents.

After warming to room temperature, inspection of the testing setup revealed a magnetized RF cable along the cavity exterior, with magnetic field up to 350 mG. The high magnetic field at the cavity wall is linked to the Q-slope and underscores the importance of 'magnetic hygiene' for Nb_3Sn cavities. Following the first test, all potentially ferrous materials in the test cryostat were verified to have fields at the surface $\leqslant$10 mG. This magnetized cable was not present during the bare niobium cavity cold test.

After cable replacement, 4.4 K tests showed high Q_0 over a broad E_{ACC} range. The low-field was $Q > 10^{10}$ with only a small slope up to $E_{\mathrm{ACC}} \approx 10\,\mathrm{MV\,m^{-1}}$. We reached $E_{\mathrm{ACC}} = 13.9\,\mathrm{MV\,m^{-1}}$ ($B_{\mathrm{PEAK}} = 105$ mT). The Q-slope above $E_{\mathrm{ACC}} \approx 11\,\mathrm{MV\,m^{-1}}$ is not field-emission-driven, based on a maximum x-ray measurement of $3\,\mathrm{mR\,h^{-1}}$ at 40 cm from the cavity wall. The origin of this high field Q slope is still uncertain, perhaps limited by single defects in the coating or non-uniformities in coating thickness.

Notably, at the ATLAS design gradient, $E_{ACC} = 7.9\,MV\,m^{-1}$, power dissipated into 4.4 K liquid helium is only 400 mW.

Multipacting-though not a fundamental material limitation, but a design influenced resonance that can impose operational limitations-has been unexpectedly persistent in the coated 145 MHz cavity: a low-level barrier at $E_{ACC} \approx 10\,kV\,m^{-1}$ has not yet been conditioned. We therefore use relatively high RF power to quickly push through the low-field barrier and measure Q versus E_{ACC} at higher fields. The fixed drive-probe coupling ($Q_{ext} = 9.5 \times 10^9$) may be insufficient and future Nb_3Sn tests will employ an adjustable power coupler.

4. Frequency tuning

Cavities in ATLAS and in any accelerator with phase-locked RF systems must be tunable. For Nb cavities, this is a multistep process. Cavities are coarse-tuned during fabrication by plastic deformation (stretching or squeezing) to bring the frequency within the range of a slow tuner. Slow tuners are usually mechanical, integrated into the cavity and cryomodule, and adjust the cavity frequency during (4.4 K) operation. A Nb cavity that is out of the slow tuner's range can be warmed to room temperature and coarse-tuned with no practical impact on field performance. Unlike niobium, Nb_3Sn-coated SRF cavities have been shown to degrade due to mechanical tuning at room temperature, but may withstand larger tuning ranges at liquid helium temperatures [27, 28].

Brittle Nb_3Sn coatings complicate tuning because any plastic deformation must be completed before coating. The final plastic tuning must be precise enough to accommodate the unavoidable frequency shifts caused by the coating process, evacuation of the interior volume, pressurization of the exterior helium volume after installation in the cryostat, and cooldown to 4.4 K. At 4.4 K, the slow tuner must provide sufficient range to bring the cavity onto resonance at the master clock frequency while avoiding deformations large enough to damage the Nb_3Sn layer.

In our approach, we measure the 4.4 K frequency of the uncoated Nb cavity. At room temperature, we apply a controlled axial plastic deformation (squeeze or stretch along the beam-port axis) to tune toward the master frequency, guided by predicted frequency shifts for the steps above. After coating, we remeasure the 4.4 K frequency. Finally, at room temperature, we adjust the Ti frame using materials with known integrated coefficients of thermal expansion to cancel the residual frequency error. This approach minimizes total strain after coating and exploits the increase in Nb yield strength at low temperature. To avoid coupling to the Ti frame, the active tuner is mounted on top of the cavity. Small dynamic frequency corrections are made by pulling up or pushing down on the quarter-wave center conductor. By contrast, beam-port-mounted tuners (e.g. ATLAS and FRIB) operate in compression only and therefore can only lower the frequency. Figure 7 shows this pneumatic tuner integrated into the titanium cage. Tuner force-frequency data are in figure 8. Cavity performance was monitored during this test and verified no performance degradation.

Post-coating the measured 4.4 K frequency was low by 70 kHz. Achieving the required 380 μm axial stretch within the available 20 cm width of the Ti frame required a negative-CTE insert. We used non-magnetic ALLVAR alloy 30 with a fractional change of $\Delta L/L = 0.0035 \pm 0.0005$ from room temperature to 77 K-similar in magnitude but opposite in sign to that of copper. Two ALLVAR rods in the Ti frame (15.25 cm long, 1.91 cm diameter) expand by $\approx$600 μm, providing ample range. These are shown in figure 9. Small brass spacers in series with the ALLVAR trimmed the final frequency to within 2 kHz, well inside the tuner and cavity elastic range. Critically, the Q_0 versus E_{ACC} showed no degradation after tuning, as shown for the 10th and most recent test in figure 6. Tests two through nine were similar (performed to fine tune the cavity frequency), with Q_0 differing by a few percent depending on the cooldown rate through T_c.

5. Coating analysis

To understand the reasons underlying the good 145 MHz cavity performance, we examine the surface of the Nb_3Sn witness samples placed at the openings of NbTi flanges on opposite ends of the cavity and coated along with the cavity [28]. Scanning electron microscope (SEM) and energy-dispersive x-ray spectroscopy (EDS) were used to image the samples' surface, determine variation in grain sizes, and analyze chemical composition. An incident accelerating voltage of 20 kV was used in EDS, which have shown to be sufficient to determine chemical composition across Nb_3Sn layer [29]. Time-of-flight secondary ion mass spectroscopy (TOF-SIMS) was employed to determine the presence of impurities based on their

Figure 7. Fine tuning of cavity using a pneumatic bellows tied to the QWR center conductor.

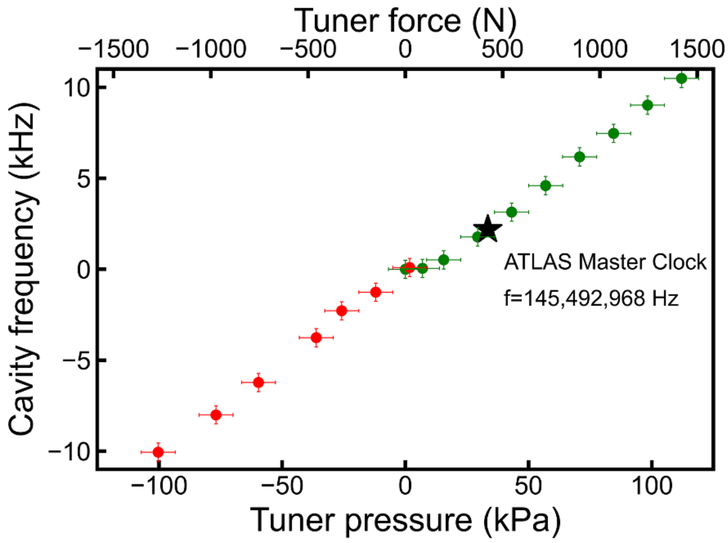

Figure 8. Cavity frequency tuning using a pneumatic push-pull tuner. Tested in both tension (green) and compression (red) modes.

charge to mass ratio (m/z), in particular, Ti, between samples. An O2+ sputter ion source with 2 kV beam energy was used to detect positive secondary ions. We used a $600 \times 600\,\mu m^2$ sputter crater and $200 \times 200\,\mu m^2$ analysis area. TOF-SIMS was complimented with EDS and confirmed by x-ray photoelectron spectroscopy (XPS) to quantify the presence of impurities on the surface of the samples.

SEM images of the samples show a uniform $\sim 1.5\,\mu m$ thick layer of Nb_3Sn with a uniform grain size of $\sim 0.8\,\mu m$. By contrast, our lower performing 218 MHz had greater end-to-end variability in grain size ($\sim 0.6 - 1.6\,\mu m$) and thickness ($\sim 1.5 - 2.7\,\mu m$). SEM images of both coating witness samples are shown in figure 10. The reasons for the film-property differences remain unclear; two new 145 MHz cavities planned for coating may help clarify these effects. The Sn content of all samples ranges between 25% and 26% as determined through EDS, which is within the range of stoichiometric Nb_3Sn composition.

We also assessed the effect of Ti, which is assumed to be detrimental to cavity performance [30]. Figure 11 shows the depth profile of Ti normalized with the Nb counts. The figure also includes the result on the witness sample of B9AS-AES002, which we refer to as baseline. This cavity showed good performance as reported in [20]. It can be observed in the figure, Ti diffused up to $\sim 1.5\,\mu m$. Within

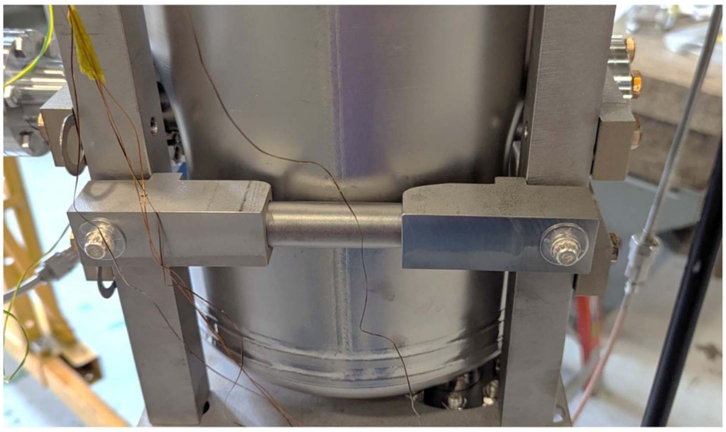

Figure 9. Coarse tuning of cavity using differential thermal expansion integrated into titanium cage.

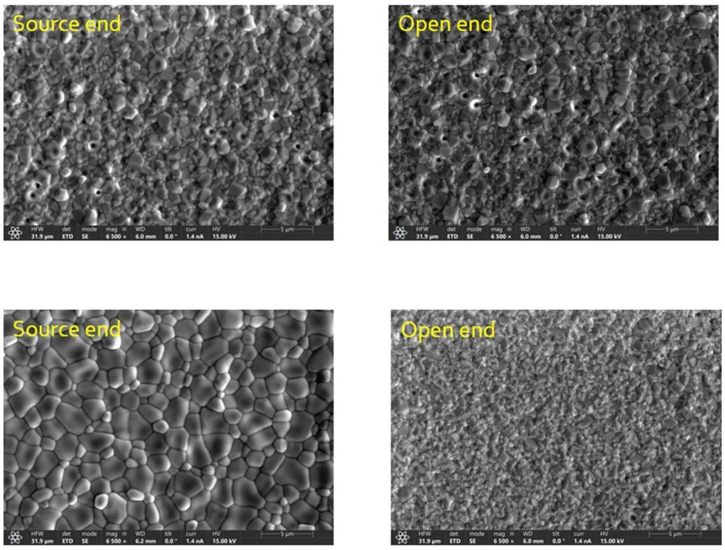

Figure 10. SEM images of witness samples for the 145 MHz coating (top) and 218 MHz coating (bottom).

$\sim$100 μm, both QWR 145 MHz and 218 MHz samples have Ti counts higher compared to baseline, with QWR 145 MHz located nearest the source as the highest. For the samples at the opposite end of the cavity, the open end of the cavity, where the magnetic field is maximum, the Ti counts are comparable. From these results, we can speculate that the Ti counts observed at levels in these Nb_3Sn witness samples do not degrade the cavity. It is worth mentioning that only traces of Ti were present since it was not detected in EDS. This has also been confirmed with XPS.

A notable difference in the coating process between 145 MHz and 218 MHz was in the modified high temperature nucleation step [20]. While the furnace temperature ramps up to 500 °C, the Sn and $SnCl_2$ source temperature is driven with high power to much higher temperatures. The high temperature nucleation creates higher vapor pressure of $SnCl_2$, which improves the uniformity of tin seeding by reducing the mean free path of the vapor and increasing the amount of Sn available at niobium surface. During 218 MHz cavity coating, the source temperature reached 600 °C during the modified high temperature nucleation step, which is only 100 °C higher than 500 °C nucleation temperature. During 145 MHz cavity coating, the source temperature reached 800 °C during the modified high temperature nucleation step, with the important difference being the rate of heating being much higher for the 145 MHz coating. We speculate the faster rate may promote tin migration and seeding of the niobium surface in the latter case.

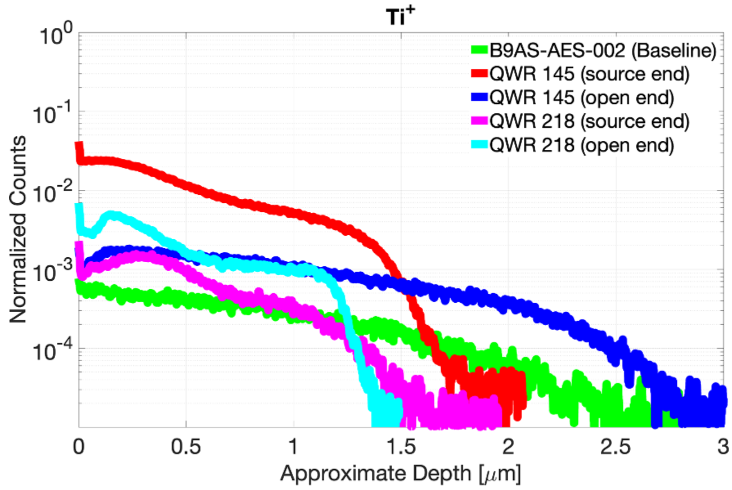

Figure 11. Titanium depth profile of witness samples compared to baseline. The counts are normalized to that of the Nb.

6. Conclusion

The peak magnetic field of 105 mT in the Nb_3Sn-coated 145 MHz cavity is among the highest fields reached in any Nb_3Sn cavity to date. The low dissipation at practical gradients together with the practical tuning system presented here demonstrate the substantial benefit of Nb_3Sn-coated low-beta SRF cavities over niobium. We plan a phased deployment of Nb_3Sn cavities in ATLAS and other ion accelerators. As a first step, the 145 MHz cavity will serve as a rebuncher at the end of the ATLAS SRF linac to deliver beams to users; successful operation would motivate a multicavity accelerating cryomodule to replace the three remaining split-ring cryomodules. Beyond ATLAS, Nb_3Sn cavities could offer significant advantages over Nb for dedicated isotope-production facilities using ion and electron linacs [31, 32] and for large proton- or light-ion SRF linacs for energy production or nuclear-waste transmutation [33].

Acknowledgment

This work is supported with resources of ANL's ATLAS facility, an Office of Science User Facilty and by the U.S. Department of Energy, Office of Nuclear Physics, under Contract No. DE-AC02-06CH11357. This manuscript has been authored by FermiForward Discovery Group, LLC under Contract No. 89243024CSC000002 with the U.S. Department of Energy, Office of Science, Office of High Energy Physics.

Data availability statement

All data that support the findings of this study are included within the article (and any supplementary files).

Author contributions

T Petersen 0009-0003-0407-3637
Conceptualization (equal), Data curation (lead), Formal analysis (equal), Funding acquisition (supporting), Investigation (equal), Methodology (equal), Project administration (equal), Writing – original draft (supporting), Writing – review & editing (equal)

G Eremeev 0000-0002-3821-1300
Conceptualization (equal), Data curation (equal), Formal analysis (equal), Funding acquisition (supporting), Investigation (equal), Methodology (equal), Writing – original draft (supporting), Writing – review & editing (equal)

B Tennis
Conceptualization (equal), Data curation (equal), Investigation (equal), Methodology (equal), Writing – review & editing (supporting)

N Tagdulang
Data curation (equal), Formal analysis (equal), Investigation (equal), Writing – review & editing (supporting)

Y Zhou
Investigation (supporting), Methodology (supporting), Writing – review & editing (supporting)

M Kedzie
Conceptualization (equal), Investigation (supporting), Methodology (supporting)

B Guilfoyle
Data curation (supporting), Investigation (supporting), Methodology (supporting)

S Xu
Data curation (equal), Investigation (supporting)

S V Kutsaev
Conceptualization (supporting), Funding acquisition (supporting), Investigation (supporting), Writing – review & editing (supporting)

R Agustsson
Investigation (equal), Methodology (equal), Writing – review & editing (supporting)

E Spranza
Investigation (equal)

P Davis
Investigation (supporting), Methodology (supporting)

G P Zinkann
Conceptualization (supporting), Investigation (supporting), Methodology (supporting)

T Reid
Investigation (equal), Methodology (equal)

S Posen
Conceptualization (supporting), Funding acquisition (supporting), Investigation (equal), Methodology (equal), Project administration (supporting), Writing – review & editing (supporting)

M P Kelly
Conceptualization (equal), Data curation (supporting), Formal analysis (equal), Funding acquisition (lead), Investigation (equal), Methodology (equal), Project administration (lead), Writing – original draft (lead), Writing – review & editing (equal)

References

[1] Mustapha B, Nolen J A, Savard G and Ostroumov P N 2017 *J. Instrum.* **12** T12002
[2] Wei J *et al* 2019 *Int. J. Mod. Phys. E* **28** 1930003
[3] Ostroumov P N, Fukushima K, Hwang K, Maruta T, Plastun A, Wei J, Zhang T and Zhao Q 2024 *J. Phys.: Conf. Ser.* **2687** 052012
[4] Aït Abderrahim H, Baeten P, De Bruyn D and Fernandez R 2012 *Energy Convers. Manage.* **63** 4
[5] Schweika W, Lindroos M, Zanini L and Ekelöf T 2023 *EPJ Web Conf.* **286** 01002
[6] Kelly M 2012 *Rev. Accel. Sci. Technol.* **5** 185
[7] Petersen T B, Kelly M P, Reid T, Kedzie M, Guilfoyle B, Chen G, Posen S, Tennis B and Eremeev G 2023 Demonstration of niobium tin in 218 MHz low-beta quarter wave accelerator cavity *Proc. Conf.* (Argonne National Laboratory and Fermi National Accelerator Laboratory)
[8] Valente-Feliciano A-M 2016 *Supercond. Sci. Technol.* **29** 113002
[9] Posen S and Hall D L 2017 *Supercond. Sci. Technol.* **30** 033004
[10] Bardeen J, Cooper L N and Schrieffer J R 1957 *Phys. Rev.* **108** 1175
[11] Padamsee H, Knobloch J and Hays T 2008 *RF Superconductivity for Accelerators* (Wiley)
[12] Posen S and Liepe M 2014 *Phys. Rev. ST Accel. Beams* **17** 112001
[13] Kutsaev S V *et al* 2020 Design of stand-alone cryomodule based on superconducting quarter-wave resonator *IEEE Trans. Appl. Supercond.* **30** 1–11
[14] Schillaci A *et al* 2025 Compact cryomodule for mobile stand-alone superconducting industrial accelerators *Cryogenics* **149** 104083
[15] Dhuley R C, Posen S, Geelhoed M I, Prokofiev O and Thangaraj J C T 2020 *Supercond. Sci. Technol.* **33** 06LT01

[16] Stilin N A, Holic A, Liepe M, Porter R D, Sears J and Sun Z 2023 *Eng. Res. Express* **5** 025078
[17] Yang Z *et al* 2024 *Supercond. Sci. Technol.* **38** 015009
[18] Ostroumov P N and Shepard K W 2001 *Phys. Rev. ST Accel. Beams* **4** 110101
[19] Conway Z A, Kelly M P and Ostroumov P N 2015 *Nucl. Instrum. Methods Phys. Res. B* **350** 94
[20] Posen S, Lee J, Seidman D N, Romanenko A, Tennis B, Melnychuk O S and Sergatskov D A 2021 *Supercond. Sci. Technol.* **34** 025007
[21] Posen S *et al* 2019 *Phys. Rev. Accel. Beams* **22** 032001
[22] Longuevergne D and Miyazaki A 2021 *Phys. Rev. Accel. Beams* **24** 083101
[23] Okada T, Kako E, Masuzawa M, Sakai H, Ueki R, Umemori K and Tajima T 2022 *Phys. Rev. Accel. Beams* **25** 082002
[24] Hall D L, Liepe M, Porter R D, Liarte D B and Sethna J P 2017 *Proc. SRF'17*
[25] Hall D L *et al* 2017 *Proc. IPAC'17*
[26] Hall D 2017 New insights into the limitations on the efficiency and achievable gradients in Nb_3Sn SRF cavities *PhD Thesis*
[27] Eremeev G V, Crahen W, Henry J, Marhauser F, Pudasaini U and Reece C E 2019 RF performance sensitivity to tuning of Nb_3Sn coated CEBAF cavities *Proc. SRF'19* pp 55–59
[28] Posen S *et al* 2019 Nb3Sn at fermilab: exploring performance *Proc. SRF'19* pp 818–22
[29] Trenikhina Y, Posen S, Romanenko A, Sardela M, Zuo J, Hall D and Liepe M 2018 *Supercond. Sci. Technol.* **31** 015004
[30] Pudasaini U, Kelley M, Eremeev G, Reece C and Tuggle J 2017 Surface studies of Nb_3Sn coated samples prepared under different coating conditions *Proc. 18th Int. Conf. RF Superconductivity (SRF'17)* pp 894–9
[31] Bollen G *et al* 2019 *Proc. Natl Acad. Sci. USA* **116** 15535
[32] Laxdal R E 2015 *Rev. Accel. Sci. Technol.* **8** 187
[33] Aït Abderrahim H 2017 *EPJ Web Conf.* **146** 01001